Electronic Supplementary Material (ESI) for Journal of Materials Chemistry B.

Supporting Information

Bio-inspired highly flexible dual-mode electronic cilia

Ya-Feng Liu, Ya-Fei Fu, Yuan-Qing Li, Pei Huang, Chao-He Xu, Ning Hu, Shao-Yun Fu**

Table S1. Comparison of the present cilia sensor with existing piezoresistive sensors and magnetic sensors

Type	Pressure sensitivity (% Pa^{-1})	LOD (Pa)	Magnetic sensitivity (T^{-1})	Ref. No.
Single model	0.77	1	NA	1
Single model	0.0001~0.001	NA	NA	2
Single model	0.22~0.604	NA	NA	3
Single model	1.51	0.2	NA	4
Single model	0.114	13	NA	5
Single model	0.06~0.08	NA	NA	6
Single model	0.015~0.055	3	NA	7
Single model	0.85	1	NA	8
Single model	0.01~1.72	NA	NA	9
Single model	0.092~16.16	NA	NA	10
Single model	NA	5	NA	11
Single model	NA	NA	100	12
Single model	NA	NA	21.3	13
Single model	NA	NA	0.93	14
Single model	NA	NA	1	15
Single model	NA	NA	0.0011	16
Dual model	0.00004~0.000074	1310	8	17
Dual model	0.025~0.4	0.9	12.08	Present

Note: NA indicates not available.

It is clear from Table S1 that the present sensor has advantages over existing piezoresistive sensors and magnetic sensors. Most of existing sensors are either single modular or are not highly sensitive. The present dual-mode sensor possesses either high sensitivities as both pressure sensor and magnetic sensor and also a very low LOD. A complicated magnetic sensor was presented previously [S12]. Its magnetic sensor shows somewhat higher magnetic sensitivity but it is only single modular with no capability in sensing pressure.

Note S1. Detailed procedure of graphene oxide (GO) coating and reduction

GO was coated on the surface of CAs by soaking of the CA film in 0.3 g/L GO solution for 5 minutes. Then, the GO coated CA film was dried in vacuum at 90 ℃ for 1 h. To avoid the deflection of CA, the GO coated CA was placed under a strong magnetic field. Afterwards, the GCCA film was obtained by reducing the GO coated CA film in 45% HI for 2 minutes. The conductivity of the GCCA film can be further improved by repeating the whole procedure.

Note S2. Theoretical prediction of the critical stress and relative resistance change

The cilia can be considered as cantilever column under a uniaxial load. The GCCA is deflected under compression, and it will be back to their initial position after the applied load released. The GCCA stays at elastic stage and the axial deformation in the bending process is very small and can thus be neglected. So, the basic assumptions are that the deformation is elastic, the cantilever column is inextensible and the flexural rigidity is constant. The schematic showing of cilia deformation is presented in Figure S5 and the exact differential equation of the deflection curve is then given by

$$\begin{cases} EI\dfrac{d\theta}{ds} = -Fy \\ \dfrac{dx}{ds} = \cos\theta \\ \dfrac{dy}{ds} = \sin\theta \end{cases} \tag{S1 a-c}$$

where θ (s) is the slope of any point along the arc length with respect to the x-axis and s is the arc length measured from the free end. S1a, S1b, S1c represent the three equations in order. The second order differential equation is given by taking the arc length's derivative of equation (S1a)

$$\frac{d^2\theta}{ds^2} = -\frac{F}{EI}\sin\theta \tag{S2}$$

Let $k^2 = F / EI$ (for a circular cross section, the moment of inertia is $I = \pi d^4 / 64$), integration of θ on both sides of equation S2 gives

$$\frac{1}{2}(\frac{d\theta}{ds})^2 = k^2\cos\theta + C \tag{S3}$$

The boundary conditions are:

$$\begin{cases} \dfrac{d\theta}{ds} = 0 \\ \theta = \alpha \end{cases} \tag{S4}$$

By applying the above boundary conditions, we can then obtain

$$ds = -\frac{d\theta}{k\sqrt{2}\sqrt{\cos\theta - \cos\alpha}}$$

Finally, we obtain

$$l = \int ds = \frac{1}{2k}\int_0^{\alpha} \frac{d\theta}{\sqrt{\sin^2\frac{\alpha}{2} - \sin^2\frac{\theta}{2}}}$$

where l is the length of cilia. Let $p = \sin\frac{\alpha}{2}$, and a new variable φ is introduced and $\sin\frac{\theta}{2} = p\sin\varphi$, then we get

$$l = \frac{1}{k}\int_0^{\pi/2} \frac{d\varphi}{\sqrt{1 - p^2\sin^2\varphi}} = \frac{1}{k}K(p) \tag{S5}$$

where $K(p)$ is complete elliptic integral of the first kind. And $K(p)$=1.8541 can be obtained at $\alpha = \pi/2$ to be shown below.

Critical stress σ_{crit}:

The critical stress is obtained at $\alpha = \pi/2$ and $l' = l_0$. According to the formula (S5), we obtain

$k = \frac{1}{l}K(p)$, for $k^2 = F/EI$

We further obtain

$$F = \left[\frac{K(p)}{l}\right]^2 EI$$

For the whole sensor, the critical load is given by

$$F_{Total} = \left[\frac{K(p)}{l}\right]^2 EI \cdot n$$

where n is the number of cilia and $n=\rho$ S, ρ is the density of CA and S is area of sensor.

Therefore, the critical stress is

$$\sigma_{crit} = \frac{F_{Total}}{S} = \frac{\left[\frac{K(p)}{l}\right]^2 EI \cdot n}{S} \tag{S6}$$

Thus, $K(p)$=1.8541 is obtained at $\alpha = \pi/2$. The average diameter and length of the CAs measured are 55 and 750 μm, respectively. The number density of CAs measured is about

1040 cm^{-2}. The Young's modulus (E) of CAs is about 3.7 MPa obtained from its stress-strain curve (Figure S4). For one circular cross section, the moment of inertia is $I=d^4/64=4.49\times10^{-19}$. Therefore, the theoretical critical stress can be estimated to be ca. 103 Pa in terms of equation S6. In the stress range of 0-103 Pa, the total resistance of the sensor decreases rapidly with increasing the pressure due to the conducting path number increases quickly. As the pressure increases, most cilia of the GCCA in the sensor were contacted with the electrodes, the largely increased contact area between the electronic cilia and the electrodes is turned to play the dominant role.

Relative change of resistance and stress:

The change of resistance is mainly controlled by the increase of the contact area S at $\sigma \geq 103$ Pa. The contact resistance is inversely proportional to the contact area, that is

$$R \propto \frac{1}{S} \propto \frac{1}{l^*}$$

where l^* is the contact length. Then, we can obtain

$$\frac{\Delta R}{R_0} \propto \frac{l^*}{l_0} = \frac{l_0 - l'}{l_0} = 1 - \frac{l'}{l_0}$$

Thus, the relative change of the resistance can be written as

$$\frac{\Delta R}{R_0} = a(1 - \frac{l'}{l_0}) + b$$

Considering $l = \frac{1}{k} K(p)$ and $k^2 = F / EI$, we obtain

$$\frac{\Delta R}{R_0} = a \cdot (1 - \frac{K(p)}{kl_0}) + b = a \cdot (1 - \frac{K(p)}{l_0} \sqrt{\frac{EIn}{S}} \frac{1}{\sqrt{\sigma}}) + b$$

Since the conducting path number results from the contact area increase, it is reasonable to generalize the above formula in the range of 0−103 Pa. Meanwhile, taking into account the mathematical significance, we obtain

$$\frac{\Delta R}{R_0} = a \cdot (1 - \frac{K(p)}{l_0} \sqrt{\frac{EIn}{S}} \frac{1}{\sqrt{\sigma + c}}) + b \tag{S7}$$

The boundary conditions are

$$\begin{cases} \frac{\Delta R}{R_0} = 0, \sigma = 0(Pa) \\ \frac{\Delta R}{R_0} = 0.4, \sigma = 103(Pa) \\ \frac{\Delta R}{R_0} = 0.66, \sigma = 1000(Pa) \end{cases}$$

We obtain

$$\frac{\Delta R}{R_0} = 0.47 \times \left(1 - \frac{10.08}{\sqrt{\sigma + 34.99}}\right) + 0.33 \qquad \text{(S8)}$$

The comparison between theoretical prediction and experiment results for the response of the GCAA sensor to the pressure applied is shown in Figure 2.

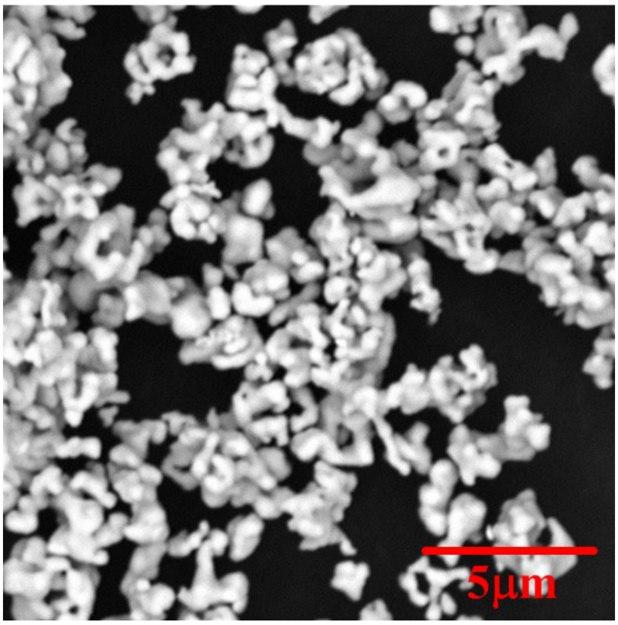

Figure S1. SEM image of Co sub-microsized particles with an average diameter of about 500 nm.

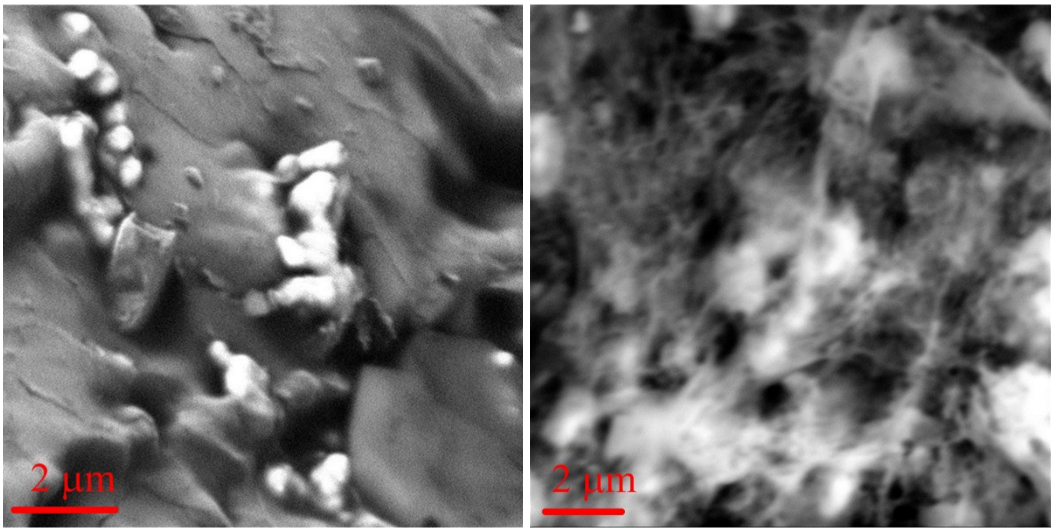

Figure S2. High magnification SEM images of the surfaces of one CA (left) and one GCCA (right).

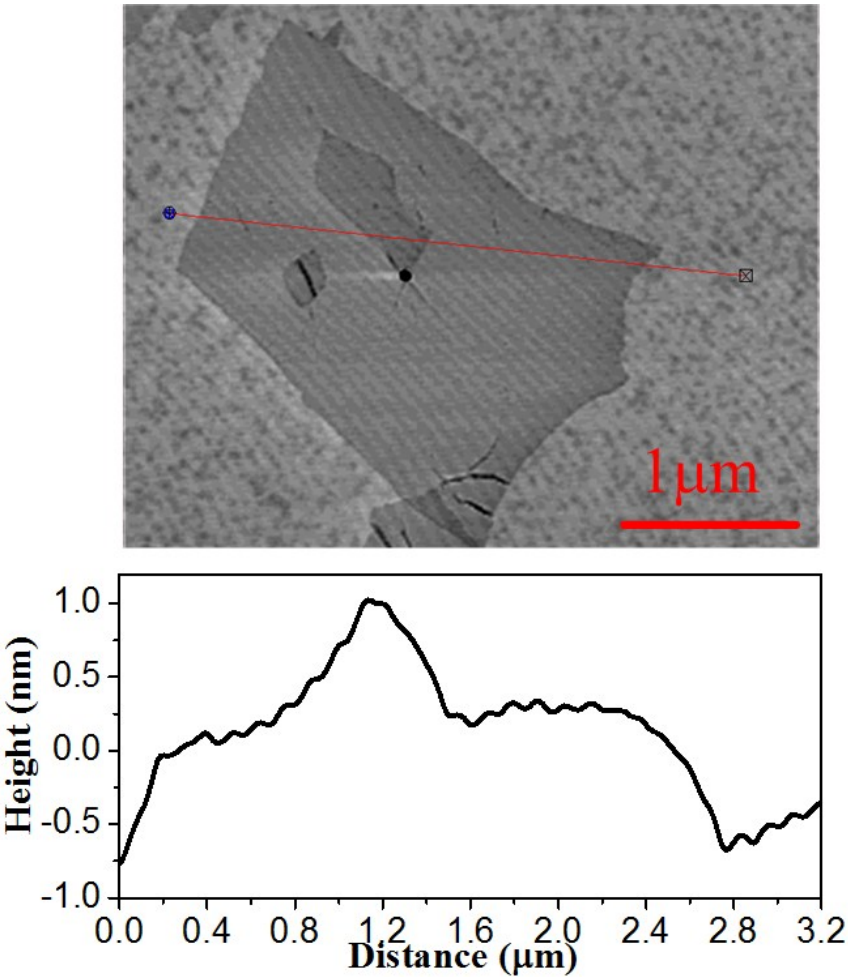

Figure S3. AFM image of graphene oxide sheets and AFM height profile.

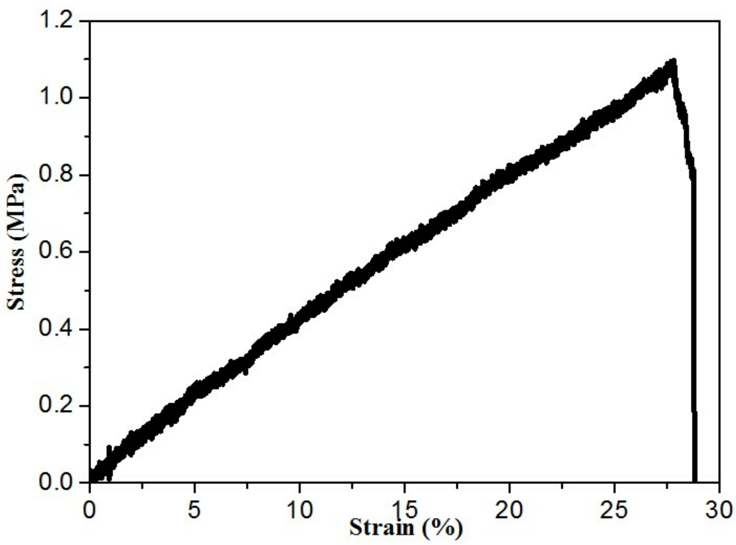

Figure S4. Typical tensile stress-strain curve of the GCCA film and the Young's modulus calculated is 3.7 MPa.

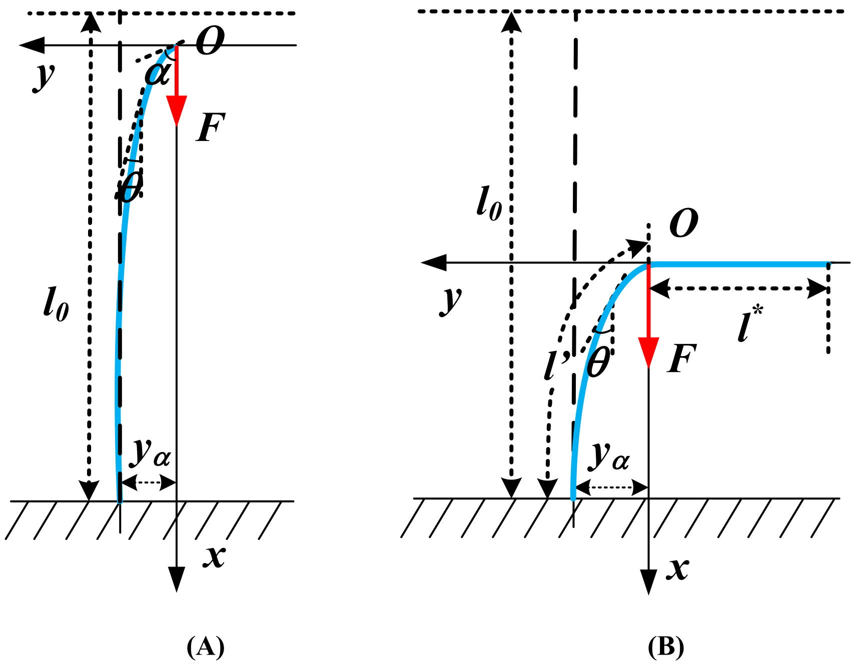

Figure S5. Schematic showing of cilia deformation under an applied force F. (A) one cilia under no pressure and (B) the cilia under an applied pressure F.

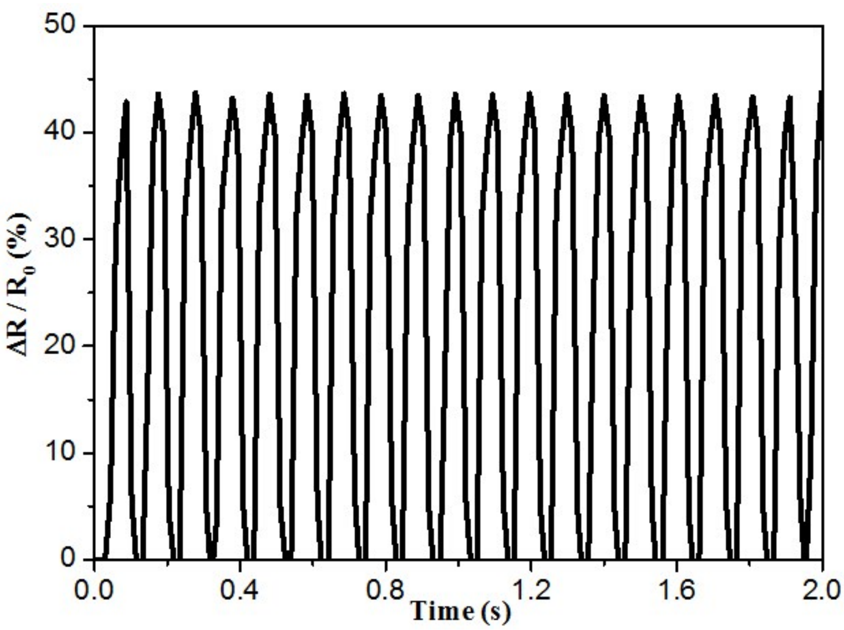

Figure S6. The RCR response of the EC sensor to compressive loading-unloading cycles with with a peak stress of 200 Pa and frequency of 10 Hz.

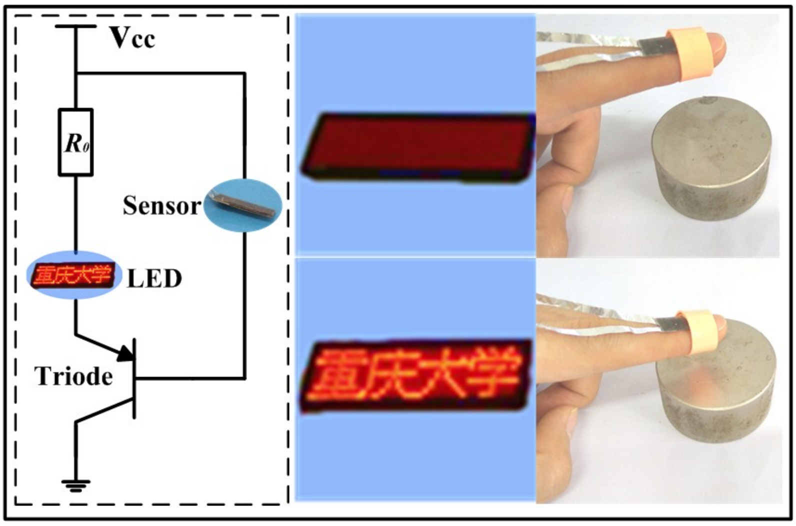

Figure S7. The magnetic field switch based on the EC-based sensor. The LED indicator is powered off when a wearer of the sensor is far away from a magnet and the LED indicator is powered on when a wearer of the sensor is approaching the magnet.

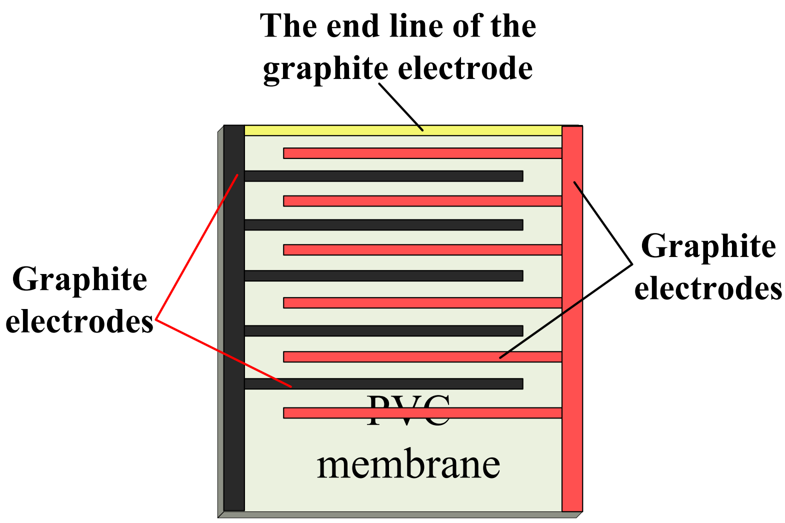

Figure S8. The pattern of graphite electrodes constructed on PVC film. The graphite electrodes were made by drawing with an 8B pencil under the assistance of a patterned model The end line of the graphite electrode was connected to achieve a limited initial resistance R_0.

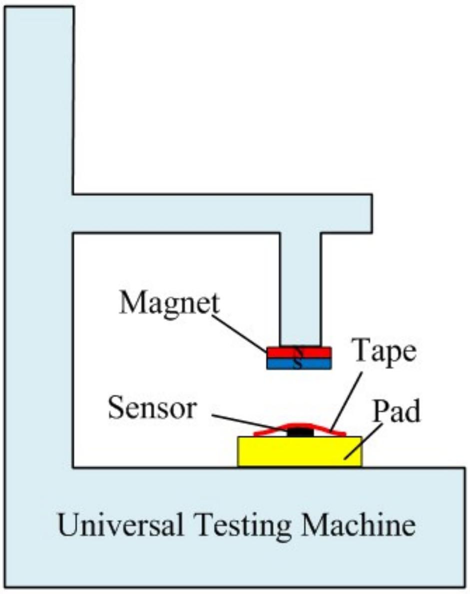

Figure S9. The response of the EC-based to an applied magnetic field yielded from the magnet fixed on the jaw of universal testing machine (UTM).

Supplementary Videos

Video S1| Visualized pressure indicator.

Video S2| Visualized magnetic field indicator.

References

[1] L. Pan, A. Chortos, G. Yu, Y. Wang, S. I saacson, R. Allen, Y. Shi, R. Dauskardt and Z. Bao, *Nat. Commun.* 2014, **5**, 3002.

[2] A. P. Gerratt, H. O. Michaud and S. P. Lacour, *Adv. Funct. Materials.* 2015, **25**, 2287.

[3] Y. Q. Li, Y. A. Samad and K. Liao, *J. Mater. Chem. A.* 2015, **3**, 2181.

[4] J. Park, Y. Lee, J. Hong, M. Ha, Jung, D. Y. H. Lim, S. Y. Kim and H. Ko, *ACS Nano*. 2014, **8**, 4689.

[5] S. Gong, W. Schwalb, Y. Wang, Y. Chen, Y. Tang, J. Si, B. Shirinzadeh and W. Cheng, *Nat. Commun.* 2014, **5**, 3132.

[6] Y. A. Samad, Y. Li, S. M. Alhassan and K. Liao, *ACS Appl. Mater. Interfaces*. 2015, **7**, 9195.

[7] S. C. Mannsfeld, B. C. Tee, R. M. Stoltenberg, C. V. Chen, S. Barman, B. V. Muir, A. N. Sokolov, C. Reese and Z. Bao, *Nat. Mater.* 2010, **9**, 859.

[8] G. Y. Bae, S. W. Pak, D. Kim, G. Lee, H. Kim do, Y. Chung and K. Cho, *Adv Mater*, 2016, **28**, 5300 .

[9] L. Q. Tao, K. N. Zhang, H. Tian, Y. Liu, D. Y. Wang, Y. Q. Chen, Y. Yang and T. L. Ren, *ACS nano*, 2017, **11**, 8790.

[10] L. Sheng, Y. Liang, L. Jiang, Q. Wang, T. Wei, L. Qu and Z. Fan, *Adv. Funct. Materials*, 2015, **25**, 6545.

[11] C. Pang, G. Y. Lee, T. I. Kim, S. M. Kim, H. N. Kim, S. H. Ahn and K. Y. Suh, *Nat. Mater.* 2012, **11**, 795.

[12] G. Lin,; D. Makarov, M. Melzer, W. Si, C. Yan and O. G. Schmidt, *Lab on a chip*. 2014, **14**, 4050.

[13] M. Pannetier, C. Fermon, G. L. Goff, J. Simola and E. Kerr, *Science*. 2004, **304**, 1648.

[14] D. Karnaushenko, D. Makarov, M. Stober D. D. Karnaushenko, S. Baunack and O. G. Schmidt, *Adv. Mater*. 2015, **27**, 880.

[15] J. Bai, R. Cheng, F. Xiu, L. Liao, M. Wang, A. Shailos, K. L. Wang, Y. Huang and X. Duan, *Nat. Nanotech.* 2010, **5**, 655.

[16] H. Gu, J. Guo, H. Wei, S. Guo, J. Liu, Y. Huang, M. A. Khan, X. Wang, D. P. Young, S. Wei and Z. Guo, *Adv. Mater.* 2015, **27**, 6277.

[17] A. Alfadhel, M. A. Khan, S. Cardoso, D. Leitao and J. Kosel, *Sensors.* 2016, **16**, 650.